A CHARACTERISTIC TRANSMISSION SPECTRUM DOMINATED BY H_2O APPLIES TO THE MAJORITY OF *HST*/WFC3 EXOPLANET OBSERVATIONS

Aishwarya R. Iyer[1,2], Mark R. Swain[1], Robert T. Zellem[1], Michael R. Line[3], Gael Roudier[1], Graça Rocha[1], and John H. Livingston[1]

Published 2016 May 27 •

The Astrophysical Journal, Volume 823, Number 2

aishwarya.iyer@jpl.nasa.gov

mark.r.swain@jpl.nasa.gov

[1] Jet Propulsion Laboratory, California Institute of Technology, 4800 Oak Grove Drive, Pasadena, CA 91109, USA

[2] California State University, Northridge, 18111 Nordhoff Street, Northridge CA 91330, USA

[3] Department of Astronomy and Astrophysics, University of California-Santa Cruz, 1156 High Street, Santa Cruz, CA 95064, USA

Received 2015 October 15
Accepted 2016 March 29
Published 2016 May 27

CrossMark

Aishwarya R. Iyer *et al* 2016 *ApJ* **823** 109

http://dx.doi.org/10.3847/0004-637X/823/2/109

methods: data analysis; planets and satellites: atmospheres; planets and satellites: general; radiative transfer

Abstract

Currently, 19 transiting exoplanets have published transmission spectra obtained with the *Hubble*/WFC3 G141 near-IR grism. Using this sample, we have undertaken a uniform analysis incorporating measurement-error debiasing of the spectral modulation due to H_2O, measured in terms of the estimated atmospheric scale height, H_s. For those planets with a reported H_2O detection (10 out of 19), the spectral modulation due to H_2O ranges from 0.9 to 2.9 H_s with a mean value of 1.8 ± 0.5 H_s. This spectral modulation is significantly less than predicted for clear atmospheres. For the group of planets in which H_2O has been detected, we find the individual spectra can be coherently averaged to produce a characteristic spectrum in which the shape, together with the spectral modulation of the sample, are consistent with a range of H_2O mixing ratios and cloud-top pressures, with a minimum H_2O mixing ratio of 17^{+12}_{-6} ppm corresponding to the cloud-free case. Using this lower limit, we show that clouds or aerosols must block at least half of the atmospheric column that would otherwise be sampled by transmission spectroscopy in the case of a cloud-free atmosphere. We conclude that terminator-region clouds with sufficient opacity to be opaque in slant-viewing geometry are common in hot Jupiters.

1. INTRODUCTION

The search for H_2O in exoplanet atmospheres has been dominated by transmission measurements obtained with space-based instruments. Although the early detections of H_2O in an exoplanet atmosphere were made with the *Hubble* and *Spitzer* instruments STIS, IRAC, and NICMOS (Tinetti et al. 2007; Barman 2008; Grillmair et al. 2008; Swain et al. 2008), the leading instrument in this area is NASA's *Hubble Space Telescope* (*HST*) Wide Field Camera 3 (WFC3) using the G141 IR grism (1.1–1.7 μm) to obtain spectra of the transit event. The scope of the collective work is impressive and constitutes the largest collection, 19, of similarly observed exoplanets presently available. These 19 transmission spectra are drawn from 16 papers by 13 authors, a majority (10 of 19) of which report a detection of H_2O (Table 1; Deming et al. 2013; Huitson et al. 2013; Line et al. 2013a; Mandell et al. 2013; Wakeford et al. 2013; Ehrenreich et al. 2014; Fraine et al. 2014; Knutson et al. 2014a, 2014b; Kreidberg et al. 2014a, 2014b, 2015; McCullough et al. 2014; Ranjan et al. 2014; Wilkins et al. 2014; Sing et al. 2015). As a whole, this sample represents a heterogeneous collection of data reduction methods, spectral resolution, observational, and model interpretation approaches. Given these differences, we focus our analysis on the H_2O absorption feature, which occurs in the near-infrared at ~1.2–1.6 μm. Here we report the trends for both spectral modulation and spectral shape and discuss the possible implications of these findings.

Table 1. *HST*/WFC3 IR Exoplanet Transmission Observations Used in This Analysis

Object Name	T_{eff} Calculated (K)	Planetary Scale Height (km)	Derived Spectral Modulation (ppm)	Derived Spectral Modulation (H_s)	Spectral Channels	Source
H_2O-detection Reported						
HAT-P-1b	1304 ± 40	544 ± 58	430 ± 178	2.8 ± 1.2	28	Wakeford et al. (2013)
HAT-P-11b	870 ± 16	269 ± 33	127 ± 47	2.2 ± 0.8	29	Fraine et al. (2014)
HD 189733b	1199 ± 21	197 ± 14	222 ± 63	2.0 ± 0.6	28	McCullough et al. (2014)
HD 209458b	1445 ± 19	558 ± 25	241 ± 38	1.5 ± 0.2	28	Deming et al. (2013)
WASP-12b	2581 ± 90	951 ± 106	280 ± 21	1.5 ± 0.1	8	Kreidberg et al. (2015)
WASP-17b	1546 ± 58	1000 ± 152	587 ± 232	1.5 ± 0.6	19	Mandell et al. (2013)
WASP-19b	2064 ± 46	502 ± 29	306 ± 86	1.5 ± 0.4	6	Huitson et al. (2013)
WASP-31b	1572 ± 35	1140 ± 105	359 ± 270	1.1 ± 0.8	25	Sing et al. (2015)
WASP-43b	1374 ± 78	97 ± 15	99 ± 66	1.4 ± 0.9	22	Kreidberg et al. (2014b)
XO-1b	1206 ± 29	275 ± 31	292 ± 110	2.7 ± 1.0	29	Deming et al.

						(2013)
Non-H_2O-detection Reported						
CoRoT-1b	1897 ± 81	598 ± 95	845 ± 959	4.1 ± 4.6	10	Ranjan et al. (2014)
CoRoT-2b	1537 ± 39	144 ± 10	95 ± 77	1.3 ± 1.0	11	Wilkins et al. (2014)
GJ 436b	649 ± 58	183 ± 20	49 ± 44	0.5 ± 0.5	28	Knutson et al. (2014a)
GJ 1214b	560 ± 29	226 ± 46	16 ± 28	0.0 ± 0.1	22	Kreidberg et al. (2014a)
GJ 3470b	651 ± 55	294 ± 88	3 ± 31	0.0 ± 0.2	107	Ehrenreich et al. (2014)
HAT-P-12b	957 ± 17	603 ± 47	0 ± 373	0.0 ± 1.1	23	Line et al. (2013a)
HD 97658b	733 ± 23	169 ± 28	22 ± 18	1.1 ± 0.9	28	Knutson et al. (2014b)
TrES-2b	1497 ± 32	269 ± 22	286 ± 162	3.0 ± 1.7	10	Ranjan et al. (2014)
TrES-4b	1784 ± 40	861 ± 95	524 ± 451	3.9 ± 3.4	10	Ranjan et al. (2014)

2. METHODS

Given a heterogeneous collection of measurements presently, we adopt a template-fitting approach to determine the spectral modulation due to H_2O opacity. We define spectral modulation as the amplitude of the H_2O feature between 1.2–1.4 μm. We generate H_2O template spectra that include the opacities due to Rayleigh scattering and H_2/H_2 and H_2/He using the CHIMERA forward model routine for transmission spectra (Line et al.

2013b; Kreidberg et al. 2014b, 2015; Swain et al. 2014) over the spectral range of the G141 grism (1.1–1.7 μm). These H_2O templates cover abundances from 0.1 to 100 ppm, the range over which the shape of the H_2O spectral modulation changes. H_2O mixing ratios below 0.1 ppm are difficult to detect and abundances above 100 ppm produce spectra that have nearly the same shape when normalized. These templates are then fit to the *HST*/WFC3 data (Figure 1) with a Levenburg–Markwardt least-squares minimization routine (e.g., Markwardt 2009) by linearly scaling the model amplitudes and vertical offsets. This exercise is carried out to debias the estimate for spectral modulation from single-point outliers and to create a consistent method to treat data reported spectral resolutions that differ by ~5.

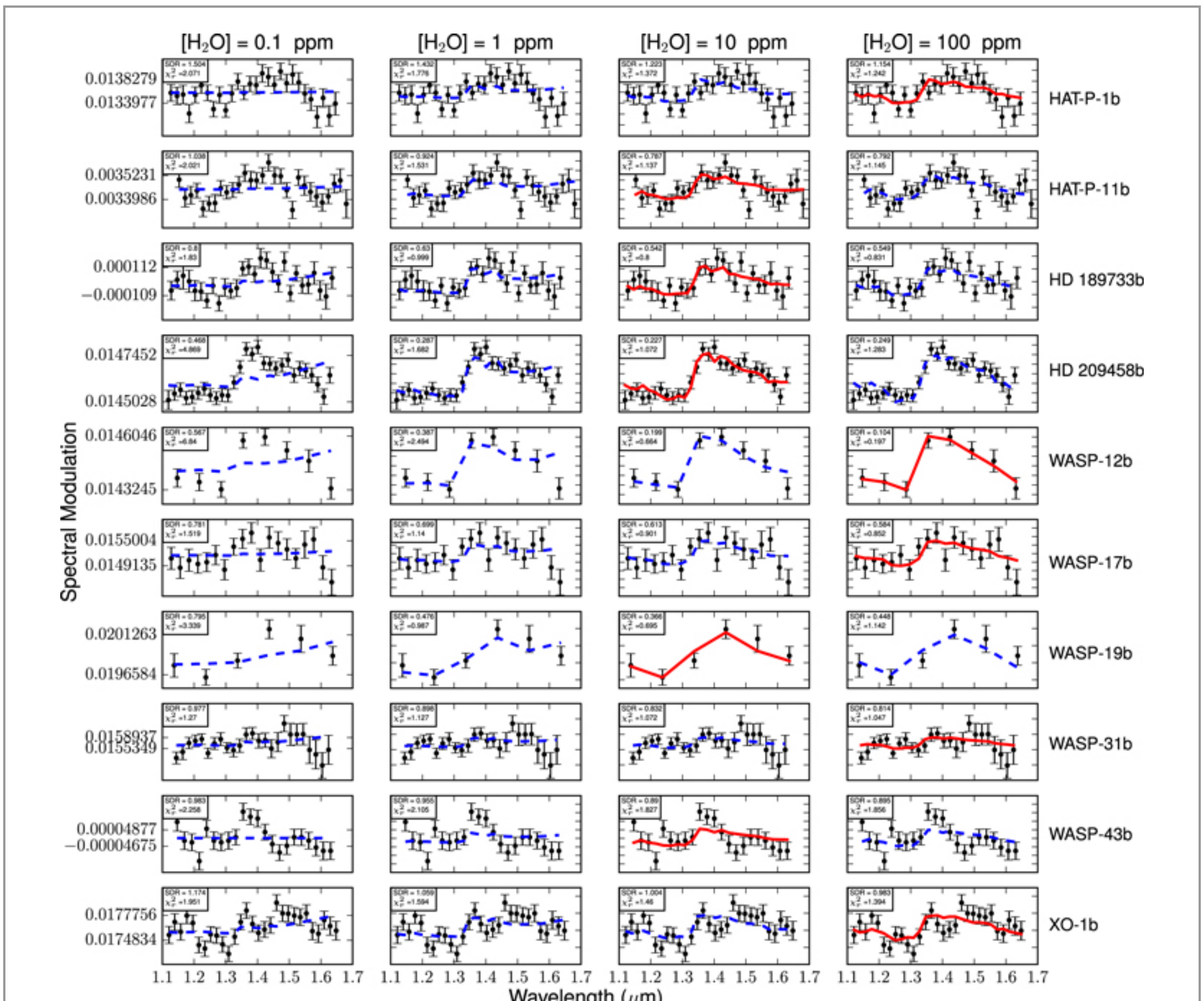

Figure 1. Ten published *HST*/WFC3 IR transmission spectra of exoplanets with a H_2O detection (the black points; Table 1) are fit to a grid of cloud-free H_2O models with abundances of 0.1, 1, 10, and 100 ppm (the blue dashed line) by scaling the model's offsets and amplitudes. The standard deviation of the residuals (SDR) in units of scale height and the reduced chi squared (χ_r^2) are noted for each case, where the minimum χ_r^2 (as well as SDR) indicates the best-fit model for each target (the solid red line). This analysis allows us to debias the estimate of the spectral modulation amplitude of the H_2O feature from outlying data points.

To facilitate further analysis, all of the *HST*/WFC3 data and their corresponding best-fit radiative transfer models are converted to units of planetary scale height H_s:

$$H_s = \frac{k_B T_{eq}}{\mu g}. \qquad (1)$$

where k_B is the Boltzmann constant, μ is the mean molecular weight of an atmosphere in solar composition (μ = 2.3 amu), g is the surface gravity, and T_{eq} is the calculated equilibrium temperature. We adopt the planetary parameters listed on exoplanets.org (Han et al. 2014) for all of these variables except the equilibrium temperature. Assuming efficient heat redistribution from the dayside to the nightside and an albedo of zero, we calculate the equilibrium temperature for each planet via the equation (Mendez 2014)

$$T_{eq} = \frac{T_* f'^{\frac{1}{4}}}{(a/R_*)^{\frac{1}{2}}} \sqrt{1 + \left(\frac{8}{\pi^2} - 1\right) e^{\frac{5}{2}}}, \qquad (2)$$

where T_* and R_* are the stellar temperature and radius, a is the semimajor axis, and e is the eccentricity.

The modulation of each planet's H_2O feature (~1.2–1.4 μm) is determined by the amplitude of the best-fit model template to prevent any outliers in each data set from skewing the spectral fit. This parameter is then plotted versus the data uncertainty, defined as the mean uncertainty in each spectra scaled by the square root of the change in resolution. The error bars on the spectral modulation are defined as the standard deviation of the residuals of the best-fit template model (Figure 2) and all values here are in units of H_s.

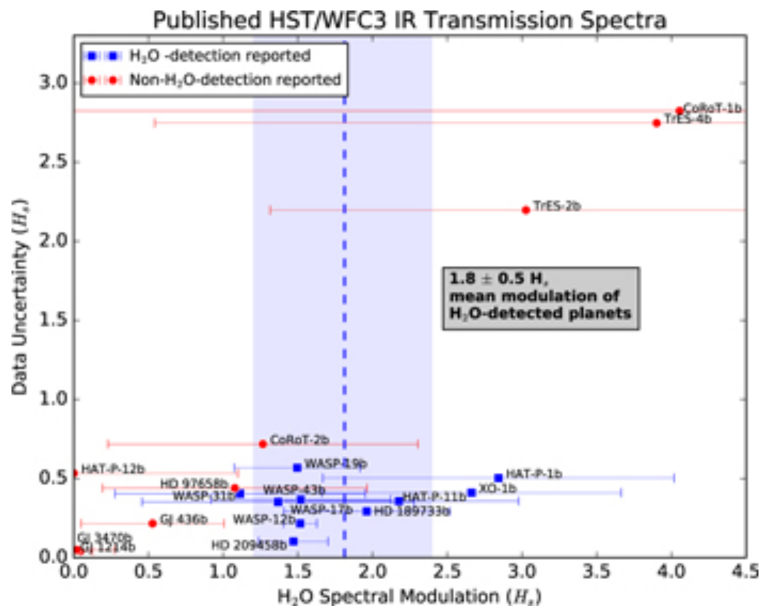

Figure 2. H_2O spectral modulation in scale heights of the 19 published *HST*/WFC3+G141 transiting exoplanet transmission spectra are plotted here vs. the uncertainty of the data. The horizontal error bars are the standard deviation of the residuals of the cloud-free H_2O model fits (see Figure 1). The exoplanets with reported H_2O detections are depicted with blue squares while reported non-H_2O-detections are red circles. We find that the H_2O-detected planets (in blue) have a mean spectral modulation of 1.8 ± 0.5 H_S; this value is smaller than the predicted spectral modulation for a clear atmosphere, suggesting that these planets have a cloud deck.

The major outlying points of TrES-2b, TrES-4b, and CoRoT-1b show a large uncertainty in their spectra as well as significant spectral modulation (Figure 2). However, their poor fit to the water templates indicate that caution should be used in interpreting modulation results for these planets.

We then search for a "representative" spectrum shared among the exoplanets published with H_2O detections. A similar approach to analyze *Spitzer* data is used by Schwartz & Cowan (2015). We construct a cumulative H_2O-detection transmission spectrum by normalizing the 10 published H_2O-detected spectra between 0 and 1, linearly interpolating them to a common wavelength grid, and then combining them with a weighted average. Unbiased uncertainties of this weighted average spectrum are calculated using the standard expression for the error in the weighted mean. The resultant spectrum (Figure 3) has a characteristic shape that is representative of this group of *HST*/WFC3 planets, with H_2O as the dominating feature.

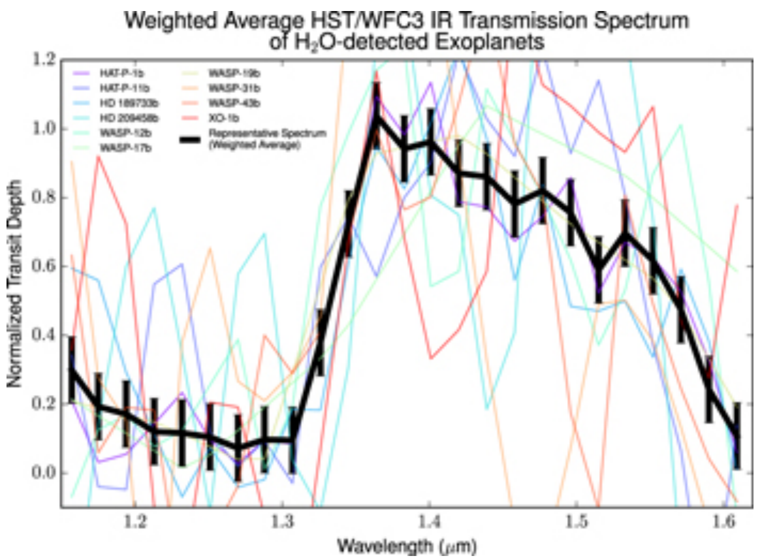

Figure 3. Normalized *HST*/WFC3 IR transmission spectra of the 10 exoplanets with reported H_2O-detections (the thin lines) are combined with a weighted mean to create a representative spectrum of H_2O-bearing exoplanets (the thick black line).

3. RESULTS AND ANALYSIS

To test the validity of this H_2O-detected "representative" spectrum and to understand the emerging patterns pertaining to this group, we compare it with four single-planet clear (cloud and haze-free) atmosphere models with H_2O abundances of 0.1, 1, 10, and 100 ppm. We include Rayleigh scattering and H_2/H_2 and H_2/He collisionally induced absorption as additional opacity sources in these models, as the planets in our sample are predominantly hot Jupiters with hydrogen and helium atmospheres. These models are also normalized between 0 and 1 to facilitate the comparison of their shape to that of the representative spectrum (the top panel of Figure 4). We find that the amplitude of the representative spectrum is consistent with H_2O abundances of 10–100 ppm.

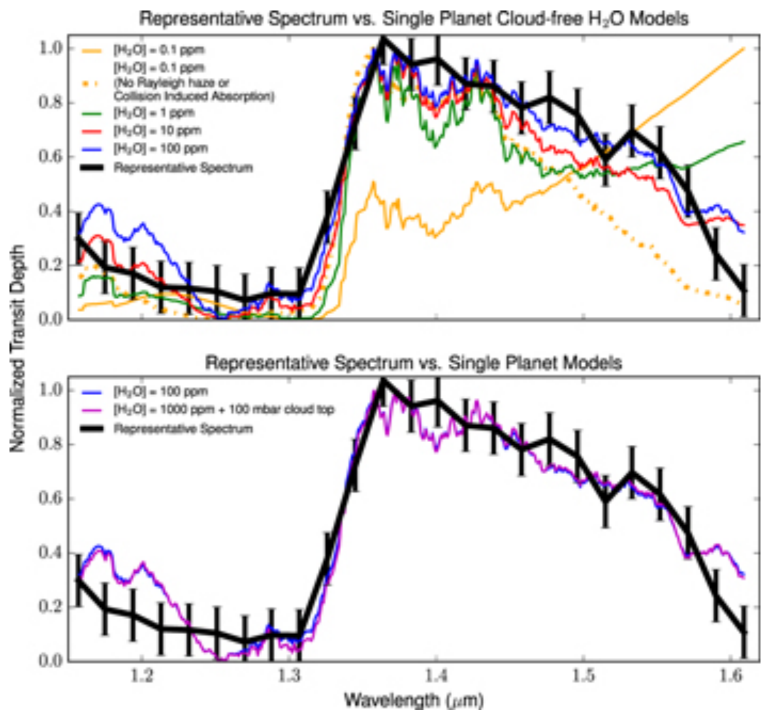

Figure 4. Single planet models with a Rayleigh haze slope of 1 (computed using Equation (1) of Lecavelier Des Etangs et al. 2008) with the CHIMERA routine (Line et al. 2013b; Kreidberg et al. 2014b, 2015; Swain et al. 2014) and assuming H_2/H_2 and H_2/He collisionally induced absorption in addition to the following. Top: cloud-free forward models of varying H_2O abundances (the thin multi-color lines) compared with the representative spectrum (the thick black line, see Figure 3). The increase in transit depth at longer wavelengths for the [H_2O] = 0.1 ppm model is due to H_2/H_2 and H_2/He collisionally induced absorption. We illustrate this effect with an [H_2O] = 0.1 ppm model without these opacity sources (the yellow dashed line). Higher H_2O abundance models have enough H_2O to mask these features, yielding a similar spectral shape when normalized. Bottom: two forward models, one cloud-free with [H_2O] = 100 ppm (the thin blue line) and the other with [H_2O] = 1000 ppm and a cloud top at 100 mbar (the thin purple line) are compared with the representative spectrum (the thick black line). These two models are nearly identical and as such fit the representative spectrum similarly well, illustrating the degeneracy of the cloud-top pressure and the water abundance.

Additionally, we also explore the effect of clouds on the H_2O spectral modulation amplitude to explain the shape of the representative spectrum. We compare the representative spectrum with a forward model with [H_2O] = 1000 ppm and a cloud top at 100 mbar, alongside a cloud-free model with [H_2O] = 100 ppm (the bottom panel of Figure 4). The choice of H_2O mixing ratio and cloud-top pressure were selected to match best to the representative spectrum. Both models show a good qualitative fit relative to the representative spectrum, indicating a degeneracy between the cloud-free and cloudy solutions.

To explore the range of values for the water mixing ratio that are consistent with the data, we perform a $\Delta\chi^2$ search of the parameter space by computing forward models and comparing their shape with the representative spectrum (the left panel of Figure 5). To generate these forward models we use parameters of a "representative planet" by computing the average T_{eq}, R_p, R_s, and log(g) of all the water-hosting planets in our sample. Cloud-free models with cloud-top pressure of ≥1 bar, where they do not interact with the transmission spectrum can be consistent with the data. Larger values for the H_2O mixing ratio can also be consistent with the data, but are degenerate with cloud-top pressure (Benneke 2015; Kreidberg et al. 2015). However, we can estimate the degree to which clouds block portions of the atmosphere that would otherwise be sampled in a transmission spectrum. Using the representative spectrum'(s) best-fit cloud-free water abundance of 17^{+12}_{-6} ppm (the left panel of Figure 5), we compute the spectral modulation for all of the planets in our sample in the following way. We run 1000 Monte-Carlo iterations per planet to generate cloud-free forward models with [H_2O] abundance sampled from the asymmetrical distribution (the left panel of Figure 5). Planet parameters of T_{eq}, R_p, R_s, and log(g) unique to each planet are used in the CHIMERA radiative transfer code (Line et al. 2013b; Kreidberg et al. 2014b, 2015; Swain et al. 2014). We then calculate the theoretical cloud-free H_2O spectral modulation derived from the MC for each planet, which is plotted against the measured spectral modulation (the right panel Figure 5). By averaging the results for the water-detected planets, we find that clouds likely remove at least half and possibly more of the observable atmospheric modulation from participating in a transit measurement.

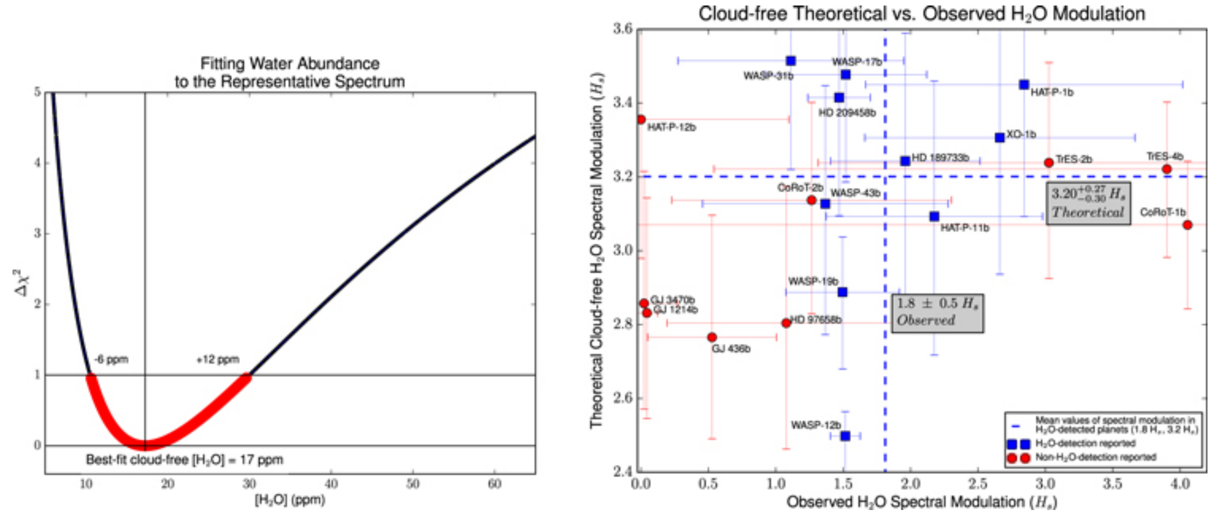

Figure 5. Left: 10,000 synthetic cloud-free spectra are generated with H_2O abundances between 1 and 1000 ppm. Each spectrum is normalized between 0 and 1 and compared with the representative spectrum (Figure 3) with a $\Delta\chi^2$ calculation. The best-fit $\Delta\chi^2$ between the synthetic data and the representative spectrum has a [H_2O]=17^{+12}_{-6} ppm. Right: clouds typically prevent at least half of the potentially measurable atmospheric annulus from being sampled in a transit measurement. We illustrate this by computing the spectral modulation for a cloud-free atmosphere using an [H_2O] abundance of 17^{+12}_{-6} ppm. Cloud-free forward models are generated for each *HST*/WFC3 planet and the observed H_2O spectral modulation is plotted vs. the theoretical pure-H_2O modulation derived from the forward models. As a whole, the H_2O-detection reported planets (the blue squares) have a mean observed modulation of 1.8 ± 0.5 H_s (Figure 2) compared with a theoretical modulation of $3.20^{+0.27}_{-0.30}$ H_s. The ratio of these values represents a maximum value (~2 H_s) of potentially viewable atmospheric column sampled by the transmission spectrum.

4. DISCUSSIONS

The H_2O spectral modulation of the *HST*/WFC3 H_2O-detected exoplanets spans 0.9–2.9 H_s with a mean modulation of 1.8 ± 0.5 H_s. This mean value differs significantly from the expectations for the cloud-free H_2O spectral modulation as compared with idealized models which predict ~7 scale heights of spectral modulation (Seager & Sasselov 2000; Brown 2001). This reduced H_2O modulation implies the presence of some additional opacity source such as clouds or aerosol haze to reduce the true spectral modulation due to H_2O. Aerosol haze has been reported in the atmosphere of the H_2O-hosting hot Jupiter, HD 189733b (Lecavelier Des Etangs et al. 2008; Pont et al. 2008; Sing et al. 2009) and clouds have been discussed by Brown (2001) and Morley et al. (2012). Quite literally, we are likely seeing the effects of H_2O above the haze and clouds, which are opaque for transit viewing geometry, but may not be so for vertical paths observed during eclipse. This hypothesis agrees with recent findings for some of the planets in our sample by Benneke (2015), Kreidberg et al. (2015), and Sing et al. (2016).

The presence of a cloud deck as a common feature of the hot Jupiter H_2O-hosting planets has implications for recent work that found a measurable difference (~100×) in the H_2O mixing ratio for the dayside and terminator regions of HD 189733b (Line et al. 2014; Madhusudhan et al. 2014). The spectral modulation due to H_2O in the terminator region is $2.0 \pm 0.5\ H_s$. In a scenario where terminator-region clouds are ubiquitous, the dayside measurement can be understood as probing a region in which dayside perpendicular viewing potentially samples 1.3 H_s of additional atmospheric path in deeper, higher-pressure regions of the atmosphere. This geometry allows for more H_2O opacity to be present in the emission spectrum and a correspondingly large value is determined for the H_2O mixing ratio.

5. CONCLUSIONS

Although we now possess the observational evidence to support the conclusion that H_2O is a common constituent in the atmospheres of hot Jupiter exoplanets, much of the water these atmospheres contain may be hidden beneath clouds. When the spectral modulation due to H_2O is measured in units of the atmospheric scale height, we find that the average H_2O-induced modulation is $1.8 \pm 0.5\ H_s$ and never exceeds 2.9 H_s. The shape of the spectral modulation is also inconsistent with extremely low H_2O abundances and suggests that a cloud layer may obscure a significant portion of the otherwise observable atmosphere. We also find that the sample of H_2O-hosting planets possesses a representative spectral shape dominated by opacity due to H_2O. The fact that the individual spectra coherently average to a consistent shape for the H_2O-hosting planets, which is reproducible with simple forward models, gives confidence that there is a representative spectrum for at least a significant portion of the hot Jupiter exoplanet population.

We are grateful to Dr. Yan Betremieux, Dr. David Crisp, Dr. Wladimir Lyra, and Dr. Yuk L. Yung for several insightful discussions on our analysis and suggestions for edits on the paper draft.

This research is based on observations made with the NASA/ESA *Hubble Space Telescope*, obtained from the Data Archive at the Space Telescope Science Institute, which is operated by the Association of Universities for Research in Astronomy, Inc., under NASA contract NAS 5-26555.

We thank the JPL Exoplanet Science Initiative for partial support of this work. The research was carried out at the Jet Propulsion Laboratory, California Institute of Technology, under a contract with the National Aeronautics and Space Administration.

This research has made use of the Exoplanet Orbit Database and the Exoplanet Data Explorer at exoplanets.org.

We thank the anonymous referee for their helpful comments.

References

↑ Barman T. S. 2008 *ApJL* **676** L61
IOPscience (http://iopscience.iop.org/1538-4357/676/1/L61) ADS

↑ Benneke B. 2015 *ApJ* submitted (arXiv:1504.07655)
Preprint

↑ Brown T. M. 2001 *ApJ* **553** 1006
IOPscience (http://iopscience.iop.org/0004-637X/553/2/1006) ADS

↑ Deming D., Wilkins A., McCullough P. *et al* 2013 *ApJ* **774** 95
IOPscience (http://iopscience.iop.org/0004-637X/774/2/95) ADS

↑ Ehrenreich D., Bonfils X., Lovis C. *et al* 2014 *A&A* **570** A89

CrossRef (http://dx.doi.org/10.1051/0004-6361/201423809) ADS

↑ Fraine J., Deming D., Benneke B. *et al* 2014 *Natur* **513** 526
CrossRef (http://dx.doi.org/10.1038/nature13785) ADS

↑ Grillmair C. J., Burrows A., Charbonneau D. *et al* 2008 *Natur* **456** 767
CrossRef (http://dx.doi.org/10.1038/nature07574) ADS

↑ Han E., Wang S. X., Wright J. T. *et al* 2014 *PASP* **126** 827
IOPscience (http://iopscience.iop.org/1538-3873/126/943/827) ADS

↑ Huitson C. M., Sing D. K., Pont F. *et al* 2013 *MNRAS* **434** 3252
CrossRef (http://dx.doi.org/10.1093/mnras/stt1243) ADS

↑ Knutson H. A., Benneke B., Deming D. and Homeier D. 2014a *Natur* **505** 66
CrossRef (http://dx.doi.org/10.1038/nature12887) ADS

↑ Knutson H. A., Dragomir D., Kreidberg L. *et al* 2014b *ApJ* **794** 155
IOPscience (http://iopscience.iop.org/0004-637X/794/2/155) ADS

↑ Kreidberg L., Bean J. L., Désert J. M. *et al* 2014a *Natur* **505** 69
CrossRef (http://dx.doi.org/10.1038/nature12888) ADS

↑ Kreidberg L., Bean J. L., Désert J. M. *et al* 2014b *ApJL* **793** L27
IOPscience (http://iopscience.iop.org/2041-8205/793/2/L27) ADS

↑ Kreidberg L., Line M. R., Bean J. L. *et al* 2015 *ApJ* **814** 66
IOPscience (http://iopscience.iop.org/0004-637X/814/1/66) ADS

↑ Lecavelier Des Etangs A., Pont F., Vidal-Madjar A. and Sing D. 2008 *A&A* **481** L83
CrossRef (http://dx.doi.org/10.1051/0004-6361:200809388) ADS

↑ Line M. R., Knutson H., Deming D., Wilkins A. and Desert J. M. 2013a *ApJ* **778** 183
IOPscience (http://iopscience.iop.org/0004-637X/778/2/183) ADS

↑ Line M. R., Knutson H., Wolf A. S. and Yung Y. L. 2014 *ApJ* **783** 70
IOPscience (http://iopscience.iop.org/0004-637X/783/2/70) ADS

↑ Line M. R., Wolf A. S., Zhang X. *et al* 2013b *ApJ* **775** 137
IOPscience (http://iopscience.iop.org/0004-637X/775/2/137) ADS

↑ Madhusudhan N., Crouzet N., McCullough P. R., Deming D. and Hedges C. 2014 *ApJL* **791** L9
IOPscience (http://iopscience.iop.org/2041-8205/791/1/L9) ADS

↑ Mandell A. M., Haynes K., Sinukoff E. *et al* 2013 *ApJ* **779** 128
IOPscience (http://iopscience.iop.org/0004-637X/779/2/128) ADS

↑ Markwardt C. B. 2009 *ASP Conf. Ser. 411, Astronomical Data Analysis Software and Systems XVIII* ed D. A. Bohlender, D. Durand and P. Dowler (San Francisco, CA: ASP) 251
ADS

↑ McCullough P. R., Crouzet N., Deming D. and Madhusudhan N. 2014 *ApJ* **791** 55
IOPscience (http://iopscience.iop.org/0004-637X/791/1/55) ADS

↑ Mendez A. 2014 *Habitable Worlds Across Time and Space* (Baltimore, MD: STScI) 32 , http://www.stsci.edu/institute/conference/habitable-worlds
ADS

↑ Morley C. V., Fortney J. J., Marley M. S. *et al* 2012 *ApJ* **756** 172
IOPscience (http://iopscience.iop.org/0004-637X/756/2/172) ADS

↑ Pont F., Knutson H., Gilliland R. L., Moutou C. and Charbonneau D. 2008 *MNRAS* **385** 109
CrossRef (http://dx.doi.org/10.1111/j.1365-2966.2008.12852.x) ADS

↑ Ranjan S., Charbonneau D., Désert J. M. *et al* 2014 *ApJ* **785** 148
IOPscience (http://iopscience.iop.org/0004-637X/785/2/148) ADS

↑ Schwartz J. C. and Cowan N. B. 2015 *MNRAS* **449** 4192
CrossRef (http://dx.doi.org/10.1093/mnras/stv470) ADS

↑ Seager S. and Sasselov D. D. 2000 *ApJ* **537** 916
IOPscience (http://iopscience.iop.org/0004-637X/537/2/916) ADS

↑ Sing D. K., Désert J. M., Lecavelier Des Etangs A. *et al* 2009 *A&A* **505** 891
CrossRef (http://dx.doi.org/10.1051/0004-6361/200912776) ADS

↑ Sing D. K., Fortney J. J., Nikolov N. *et al* 2016 *Natur* **529** 59
CrossRef (http://dx.doi.org/10.1038/nature16068) ADS

↑ Sing D. K., Wakeford H. R., Showman A. P. *et al* 2015 *MNRAS* **446** 2428

CrossRef (http://dx.doi.org/10.1093/mnras/stu2279) ADS

↑ Swain M. R., Line M. R. and Deroo P. 2014 *ApJ* **784** 133
IOPscience (http://iopscience.iop.org/0004-637X/784/2/133) ADS

↑ Swain M. R., Vasisht G. and Tinetti G. 2008 *Natur* **452** 329
CrossRef (http://dx.doi.org/10.1038/nature06823) ADS

↑ Tinetti G., Vidal-Madjar A., Liang M. C. *et al* 2007 *Natur* **448** 169
CrossRef (http://dx.doi.org/10.1038/nature06002) ADS

↑ Wakeford H. R., Sing D. K., Deming D. *et al* 2013 *MNRAS* **435** 3481
CrossRef (http://dx.doi.org/10.1093/mnras/stt1536) ADS

↑ Wilkins A. N., Deming D., Madhusudhan N. *et al* 2014 *ApJ* **783** 113
IOPscience (http://iopscience.iop.org/0004-637X/783/2/113) ADS